Climate Dynamics (1995) 12:101–112

Climate Dynamics

Quasi-quadrennial and quasi-biennial variability in the equatorial Pacific

Ning Jiang[1], J. David Neelin[1,2] and Michael Ghil[1,2]

[1] Department of Atmospheric Sciences, University of California, Los Angeles, CA 90095-1565, USA
[2] Institute of Geophysics and Planetary Physics, University of California, Los Angeles, CA 90095-1567, USA

Received: 2 December 1994 / Accepted: 28 July 1995

Abstract. Evaluation of competing El Niño/Southern Oscillation (ENSO) theories requires one to identify separate spectral peaks in equatorial wind and sea-surface temperature (SST) time series. To sharpen this identification, we examine the seasonal-to-interannual variability of these fields by the data-adaptive method of multi-channel singular spectrum analysis (M-SSA). M-SSA is applied to the equatorial band (4°N-4°S), using 1950–1990 data from the Comprehensive Ocean and Atmosphere Data Set. Two major interannual oscillations are found in the equatorial SST and surface zonal wind fields, U. The main peak is centered at about 52-months; we refer to it as the *quasi-quadrennial* (QQ) mode. *Quasi-biennial* (QB) variability is split between two modes, with periods near 28 months and 24 months. A faster, 15-month oscillation has smaller amplitude. The QQ mode dominates the variance and has the most distinct spectral peak. In time-longitude reconstructions of this mode, the SST has the form of a standing oscillation in the eastern equatorial Pacific, while the U-field is dominated by a standing oscillation pattern in the western Pacific and exhibits also slight eastward propagation in the central and western Pacific. The locations of maximum anomalies in both QB modes are similar to those of the QQ mode. Slight westward migration in SST, across the eastern and central, and eastward propagation of U, across the western and central Pacific, are found. The significant wind anomaly covers a smaller region than for the QQ. The QQ and QB modes together represent the ENSO variability well and interfere constructively during major events. The sharper definition of the QQ spectral peak and its dominance are consistent with the "devil's staircase" interaction mechanism between the annual cycle and ENSO.

Correspondence to: N. Jiang

1 Introduction and motivation

Many observational studies and model simulations during the past two decades have provided a relatively detailed description of the pattern of interannual climate variability associated with the El Niño/Southern Oscillation (ENSO) (e.g., Cane 1986; Philander 1990). Fundamental questions still remain, particularly concerning the growing evidence that multiple time scales may be involved in ENSO variability. Both power spectra of tropical time series and the evidence that warm ENSO episodes are locked to the annual cycle (Rasmusson and Carpenter 1982) hint at this. It has long been noted that individual warm events generally evolve on a time scale of about two years (Rasmusson and Carpenter 1982; Trenberth and Shin 1984; Barnett 1988). Meehl (1987) concluded that an important component of interannual variability in the low-latitude Indian Ocean-Western Pacific sector could be characterized as an alternation between "weak" and "strong" annual cycles, while Quinn et al. (1978) gave the typical separation between major ENSO warm events as 3–8 years. More recently, Lau and Sheu (1988) found evidence of a *quasi-biennial* (QB) signal in global precipitation.

Current interest in multiple ENSO time scales was whetted by Rasmusson et al. (1990), who used singular spectrum analysis (SSA) combined with conventional spectral techniques to identify low-frequency and QB peaks in wind and SST series; these authors did not explicitly associate the low-frequency mode with ENSO. Keppenne and Ghil (1992a, b) found evidence of such a split in the Southern Oscillation Index (SOI) series, while Penland et al. (1991) and Dickey et al. (1992) found it in atmospheric angular momentum and length-of-day time series. The spatial patterns associated with QB and low-frequency spectral bands (Ropelewski et al. 1992) and the nonlinear interaction between them (Barnett 1991) have been investigated by filtering in predetermined spectral bands, selected a priori to correspond to these two time scales. Recently, Latif et al. (1993, 1995 submitted) used principal oscil-

lation pattern (POP: Hasselmann 1988) analysis to extract spatial patterns of wind stress, SST and 20 °C-isotherm depth and found low-frequency and QB components in a twenty-year time series.

These studies make a plausible case for the existence of more than one basic time scale of interannual variability. The challenge now is to describe the tropical ocean-atmosphere system's behavior on such separate time scales in sufficient detail, so as to distinguish between theoretical mechanisms that could give rise to the observed peaks. In particular, the characterization of the low-frequency component remains somewhat vague, in both its temporal and spatial aspects. This study aims to verify and better quantify the hypothesized multiple scales of ENSO time series. We also discuss briefly the relationship among the interannual modes and the seasonal cycle, in the context of previous work and possible mechanistic explanations.

In Sect. 2, method, data, and computational choices are given. In Sect. 3, we apply multi-channel SSA (M-SSA) to the observational data from the Comprehensive Ocean and Atmosphere Data Set (COADS) to identify interannual variability. The behavior of each interannual mode identified in the SST and surface zonal wind fields is described in Sect. 4. In Sect. 5, we present the annual cycle's features. Concluding remarks appear in Sect. 6. The basic formulae used in M-SSA are included in the Appendix.

2 Method, data and computational choices

Since conventional spectral analysis is of limited value when applied to the relatively short and noisy time series available, we use M-SSA, which can systematically identify coherent space-time patterns (Broomhead and King 1986a, b; Vautard and Ghil 1989; Ghil and Vautard 1991; Kimoto et al. 1991; Vautard et al. 1992; Plaut and Vautard 1994) in such series. The computational procedure is summarized in the Appendix.

An advantage of M-SSA with respect to other spectral methods is that, due to its data-adaptive basis functions, it can capture an anharmonic oscillation, of possibly nonlinear origin, by a single pair of EOFs, rather than by multiple spectral peaks. Complex principal component analysis (CPCA: Horel 1984; Preisendorfer 1988) is commonly used to recognize propagating patterns; it provides an expansion similar to M-SSA, where the basis functions are EOFs, in time or space, and harmonic waves in the complementary domain (Bernardet et al. 1990). However, CPCA has difficulty separating multiple peaks when spatially similar oscillations cover a wide frequency range and in practice band-pass prefiltering is often performed (e.g., Barnett 1991). In contrast M-SSA provides a self-consistent separation in both time and space that can discriminate between multiple peaks (Plaut and Vautard 1994).

We focus on two key fields that characterize interannual variability in the tropics, sea-surface temperature (SST) and surface zonal wind (U), for which reasonably long time series are available. For a complete characterization of ENSO mechanisms, inclusion of subsurface data would be desirable (e.g., Latif et al. 1995 submitted), but the brevity of their time series restricts the accuracy with which spectral characteristics may be defined. We analyze here a 41-year set of monthly averages from the COADS data, covering the equatorial Pacific. The analyses span the time interval January 1950 to December 1990, chosen because prior to this the data set contains too many gaps.

Because the signal of greatest interest is concentrated at the equator, we consider averages over an equatorial band, 4°N to 4°S. A moving boxcar spatial average with area 8° latitude by 10° longitude centered at the equator was computed to retain sufficient longitudinal resolution, while greatly reducing data gaps. A cubic spline interpolation in time was performed to fill the few remaining gaps. Other spatial averaging intervals were used to as certain the robustness of the results, in particular 4° latitude × 2° longitude and 8° latitude × 20° longitude. In order to isolate the nearly periodic modes of the interannual variability, the seasonal cycle was removed by using the calendar-monthly mean for each spatial channel and a linear trend was removed by least-square fitting.

In the time domain, the choice of window size represents a compromise between the amount of significant information (the larger the window the better) and the statistical confidence (the smaller the window the better). Generally, one must evaluate the stable features of the eigenset by varying the window size over a range. Vautard et al.'s (1992) experiments indicated that the use of a given window size M allows the identification of oscillations with periods roughly in the range ($M/5$, M), if the time series is long enough. A window size of 61 months was chosen for the results presented in the following, i.e., periods from 1 to 5 years may be accurately distinguished; larger periods can still be found by the technique but they would not appear as separate eigenmodes. Other M-values were used to verify results (see Sect. 4.5 below).

A similar trade-off exists in the space domain between resolution (i.e., number of spatial channels) and statistical confidence. Our choice of 10°-longitude boxes was sufficient to resolve accurately the spatial scales of SST and U, while keeping the product of channels and lags sufficiently small.

In M-SSA, oscillations appear as paired eigenvalues in the singular spectrum and the associated eigenvectors and principal components (PCs) are in quadrature. Two natural criteria based on the spectral properties of the eigenvectors (Sect. 4.2 in Vautard et al. 1992) were used to select the eigenvalue pairs.

3 Identifying modes of interannual variability

The M-SSA eigenvalue spectra for SST, U, and the combined SST-U are displayed in Fig. 1a–c, up to order 60. The error in the eigenvalues was estimated with a slightly improved form of Ghil and Mo's (1991) heuristic variance formulation. The 95% confidence inter-

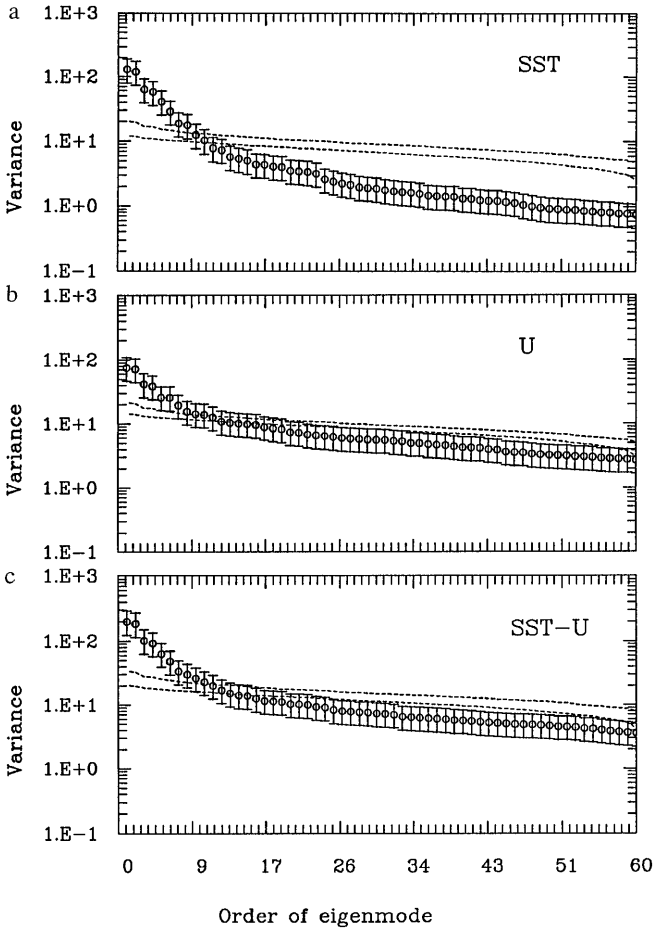

Fig. 1a–c. M-SSA eigenvalue spectra of the three calculations for **a** SST, **b** U and **c** combined SST-U, up to order 60, with error bars indicating the 95% confidence interval, plus a 95-% confidence interval from a sample of 100 Monte Carlo white-noise realizations (*dashed lines*). The individual error bars for eigenvalue λ_k were determined as $\lambda_k \pm \delta\lambda_k$, where $\delta\lambda_k = (2/N_d)^{1/2}\lambda_k$, $N_d = c(N/\tau_d)$ and τ_d represents a decorrelation time. This differs from Ghil and Mo's (1991) heuristic formula by allowing $1 \le c \le 2$, since Vautard et al. (1992) showed that the original $c = 1$ was too conservative (see also Sect. 3.2 of Unal and Ghil 1992)

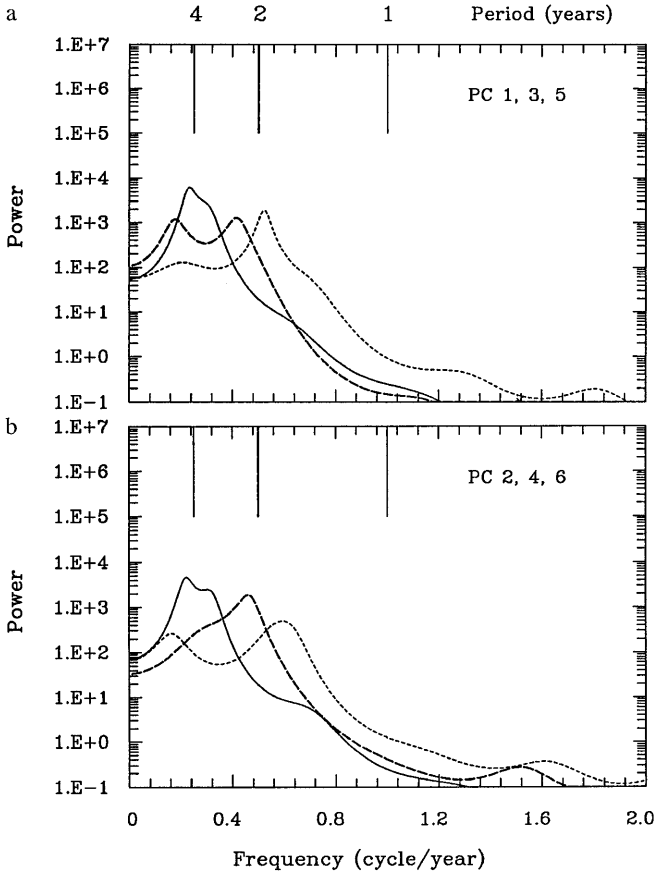

Fig. 2a, b. Maximum entropy method (MEM) spectra of SST. **a** PC 1 (*solid*), 3 (*dashed*), and 5 (*dotted*); **b** PC 2 (*solid*), 4 (*dashed*), and 6 (*dotted*). The spectral bandedness of the PCs permits the use of a low MEM order, equal to 30, which still provides high spectral resolution, while avoiding spurious peaks

val was computed using 100 Monte Carlo realizations of white noise with the same variance as the time series being analyzed. The white-noise confidence interval implies that six M-SSA components may be significant. That the spectrum of U is much flatter than that of SST indicates that the wind data are in some sense noisier, as expected from physical considerations.

A visual inspection of all the spectra suggests that some eigenvalues form pairs. The power spectra obtained using the maximum entropy method (MEM) for SST (Fig. 2) and U (Fig. 3) are shown for the leading PCs 1–6 (Penland et al. 1991; Vautard et al. 1992; Dettinger et al. 1995). As is apparent from the plots, these tend to occur in pairs with similar spectral peaks, and indeed PCs 1–2, 3–4 in SST and 1–2, 3–4, 5–6 in U pass the two pairing criteria of Vautard et al. (1992). Pair 5–6 in SST shares some common features but does not pass the two criteria. The leading pair, 1–2, gives a clear peak at just over 4 years in both fields and so we refer to this as the *quasi-quadrennial* (QQ) mode. It corresponds to the "low-frequency" mode identified by Rasmusson et al. (1990), but the peak is more sharply defined by the methodology here. The peaks associated with PCs 3–4 and 5–6 are less well separated: both have frequencies around or just over two years, so we refer to these collectively as the QB modes, following the terminology of Rasmusson and colleagues. However, it is apparent from the spectra that it is more difficult to argue conclusively for a single phenomenon with a well-defined spectral peak in this QB range. Spectra from the combined SST-U analysis resemble the univariate analysis (not shown). This similarity attests to the coherence of the oscillation in each case.

Figure 4 displays the SST and U analysis as stack spectra from the cumulative sums over PCs at various truncations; specifically, the spectra correspond to retaining spectral density associated with PCs 1–2, 1–6, 1–12 and all PCs, respectively. When all PCs are included, the spectrum very closely approximates the sum of the spectra of the individual channels of the normalized raw data. The QQ peak stands out clearly, even when the "noise" background associated with the sum over all other PCs is included. The broad peak in the QB range, associated with PCs 3–6, stands out, but

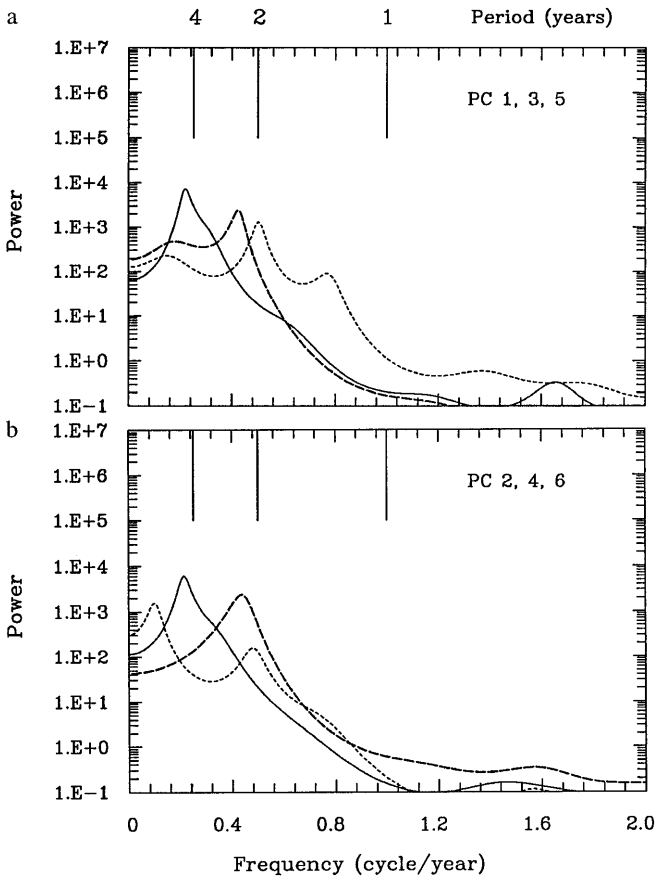

Fig. 3a, b. MEM spectra of U. **a** PC 1, 3, and 5; **b** PC 2, 4, and 6; same convention as in Fig. 2

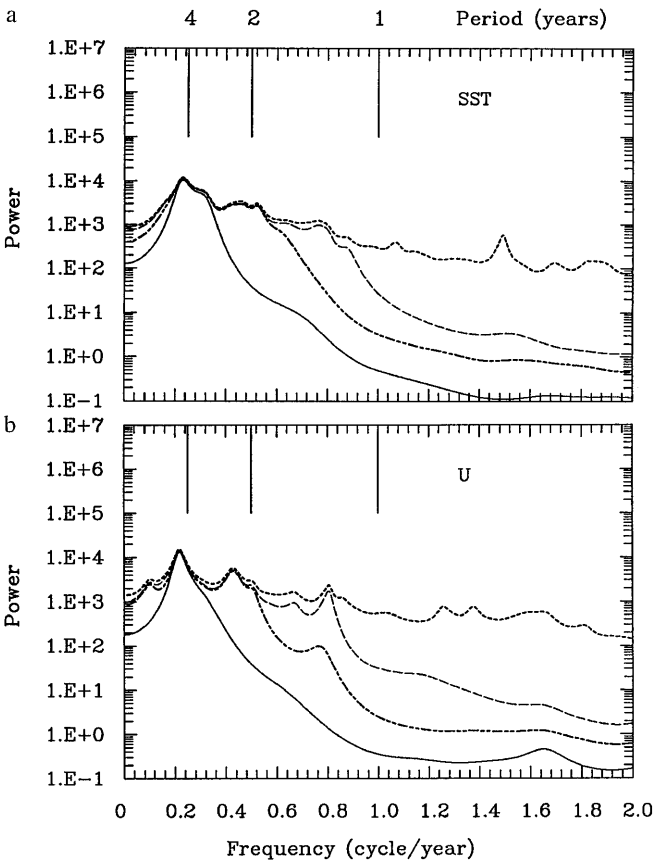

Fig. 4a, b. The stack spectra from the cumulative sums over PCs at various truncations for **a** SST and **b** U. Stack 1–2 (*solid*), 1–6 (*dash-dotted*), 1–12 (*dashed*), and complete (*dotted*)

much less clearly. A slight peak at 15–16 months may also be seen in both SST and U spectra. It is associated with PCs 7–8 in SST and 9–10 in U and in fact passes the pairing criteria. While we hesitate to place too much emphasis on it, its presence is intriguing, as will be seen from the comparison with modeling results in the discussion section.

A summary of interannual spectral peaks that pass both pairing criteria is given in Table 1. The period of the oscillation is estimated as the peak location of the sum $P_k(f)+P_{k+1}(f)$ of the MEM spectral densities of the two PCs. The variance is calculated from the eigenvalue spectrum. The QQ oscillation has remarkably similar periods in SST and U, 53 and 54 months, respectively. The amplitude is stable in the eastern and central Pacific. This mode accounts for 39% of the variance in the SST time series with trend and seasonal cycle removed. In U, it contains only 19% of the variance since the "noise" background is larger. The results from the combined SST-U analysis are consistent with the two separate ones: 52 months and 27% of variance.

The QB variance is split across two pairs with peaks at 28 and 24 months in U; similar results hold for SST but only the 28-month peak meets the pairing criteria. The one or two significant QB modes account for about half the variance of the single QQ mode in SST

Table 1. Characteristics of the oscillatory pairs identified in section 3 for the analysis with seasonal cycle removed

Variables	Pair	Period (months)	Variance (%)
SST	1– 2	53	38.7
	3– 4	28	18.8
	(5– 6)	(23)	(10.8)
	7– 8	16	5.6
U	1– 2	54	19.0
	3– 4	28	10.5
	5– 6	24	6.7
	9–10	15	3.7
SST-U combined	1– 2	52	27.2
	3– 4	28	13.8
	9–10	15	3.5

Each row corresponds to a pair of eigenvalues of index $(k, k+1)$. The pair (5–6) does not pass all the criteria for statistical significance in Sec. 2 but is included, for completeness, in parentheses. The first column gives the variable analyzed, where "combined" refers to a joint analysis of both variables. The second column gives the index number of the pair. The third column contains the period of the oscillation calculated as the peak value of the sum of the MEM spectra of the two PCs. The fourth column gives the total percentage of variance associated with the oscillatory pair, calculated from the eigenvalue spectrum

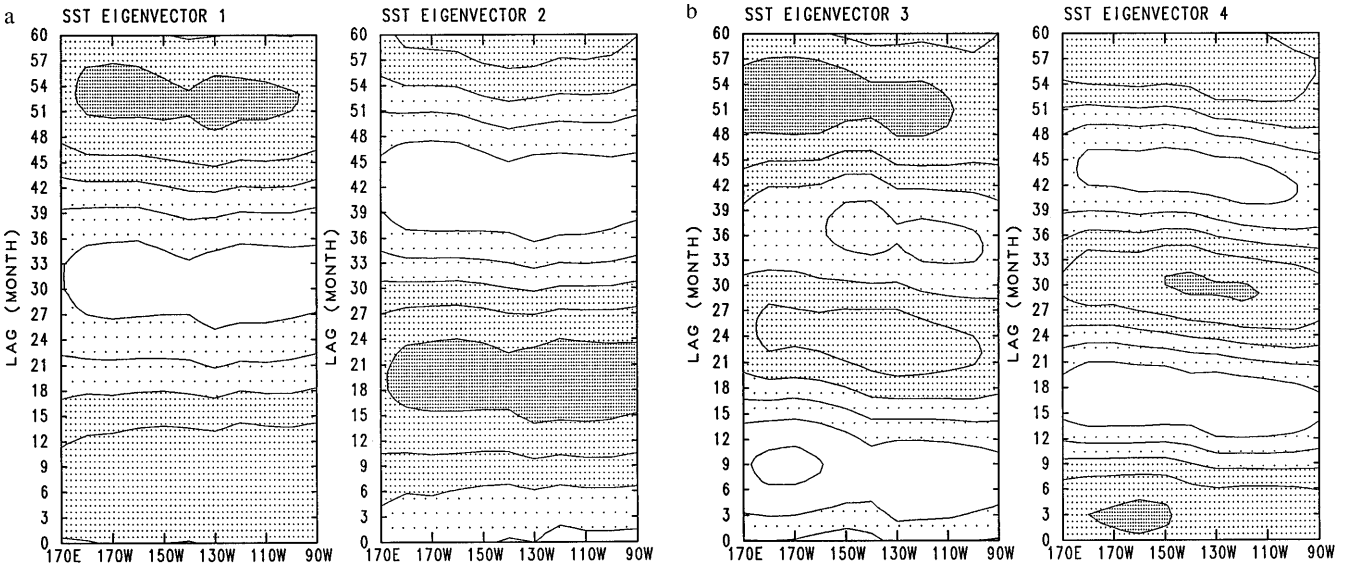

Fig. 5a, b. The pair of eigenvectors for SST associated with **a** the quasi-quadrennial (QQ) mode (1–2) and **b** the quasi-biennial (QB) mode (3–4). Contour interval is 0.025 for normalized eigenvectors (nondimensional); *darkest stippling* for regions over 0.05, *no stippling* for regions less than −0.05

and for an almost equal amount in U: 19% and 17%, respectively. Again the combined SST-U analysis is consistent with the two separate ones. This confirms further the robustness of these two oscillations in the equatorial Pacific, and serves as an indication that the two oscillations in the SST and U fields are related. While an important aspect of ENSO dynamics is missing from our analysis of surface fields, namely a measure of upper ocean dynamics, such as heat content, we note that Unal and Ghil (1995) find a period of 51 months in western Pacific sea level records, as well as a QB signal throughout the Pacific.

4 Reconstruction of the interannual variability

The M-SSA eigenvectors carry a characteristic structure in space and in time lag; two examples are shown in Fig. 5. The pair of eigenvectors for SST associated with the QQ mode (Fig. 5a) has broad spatial structure. The QQ time scale and the time-quadrature of the two members of the pair is evident. The significant pair of SST eigenvectors for the QB mode (Fig. 5b) has similar quadrature and broad spatial characteristics, with the added hint of westward propagation.

4.1 Quasi-quadrennial (QQ) time series

Even more useful than examining the eigenvectors individually or in pairs is to reconstruct the space-time series associated with each pair or subset of eigenvectors (see the Appendix). These reconstructed components (RCs) represent the contribution to the original time series of a given set of eigenelements (Ghil and Vautard 1991; Plaut and Vautard 1994). The signal associated with the pair giving the clear QQ peak is shown in Fig. 6. The RCs are displayed for the separate SST and U analysis, to provide a means of checking the results, since we have strong reasons to believe these fields must vary together.

For the SST anomaly, the QQ oscillation appears as a standing pattern. The maximum anomaly is located around 120° W. The time series also shows strong lower-frequency modulation, with quiescent and active spells. The most active spells occurred during 1957–58, 1969, 1972–73, 1982–83, and 1986–87. There is a correlation of 0.73 between the NINO-3 index (SST averaged over the region 5° N–5° S, 150° W–90° W) for the reconstructed QQ and the original time series. The QQ reconstructed signal contributes 28.5% of the NINO-3 variance. Thus the QQ described here may be regarded as the dominant ENSO mode, as it accounts for most of the ENSO variability.

For the U anomaly, the QQ mode is dominated by a standing oscillation pattern but also exhibits a slight eastward propagation in the western Pacific (e.g., Barnett 1983). The maxima are located around 170° E, as expected for ENSO-related wind anomalies. The wind time series exhibits the same epochs of strong activity as for SST, but is also active in 1952–53 when SST anomalies are present but relatively weak. Since there are strong theoretical reasons for believing the wind at low frequencies must be driven by SST anomalies, we interpret the latter as an artifact of the analysis; it is encouraging that during most active spells the agreement between the two series is good.

4.2 Quasi-biennial (QB) time series

To examine the QB variability, we choose to sum over both pairs of eigenvalues that have peaks in the QB range, i.e., modes 3–6 (Fig. 7). The SST anomaly (Fig.

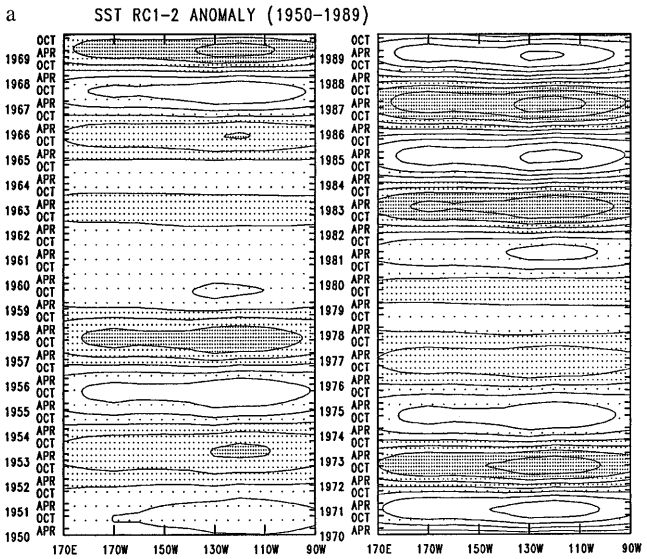

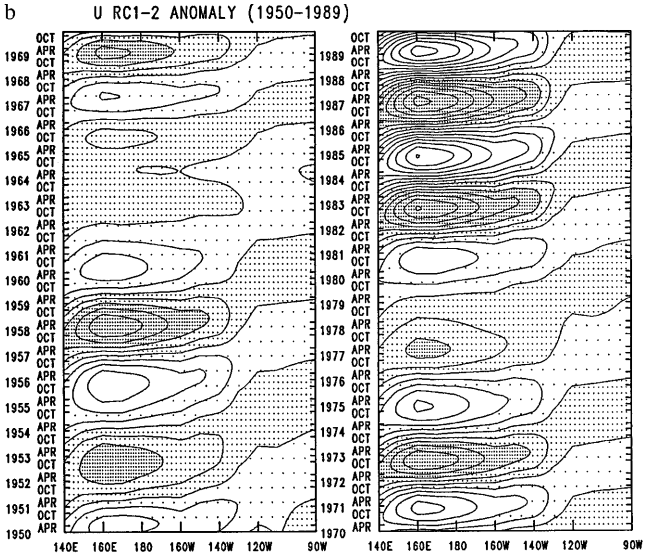

Fig. 6a, b. QQ oscillation represented by the reconstructed components (RCs) 1–2 for **a** SST. Contour interval is 0.25 °C; *darkest stippling* for regions over 0.5 °C, *no stippling* for regions less than −0.5 °C. **b** U. Contour interval is 0.25 m/s, *darkest stippling* for regions over 0.5 m/s, *no stippling* regions less than −0.5 m/s. To capture the salient features best, the domain of the U-analysis is slightly larger; results for an equally large SST domain (not shown) are similar

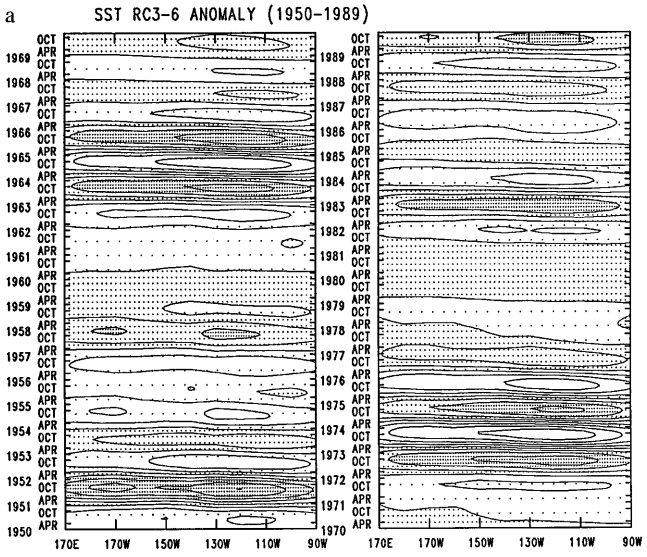

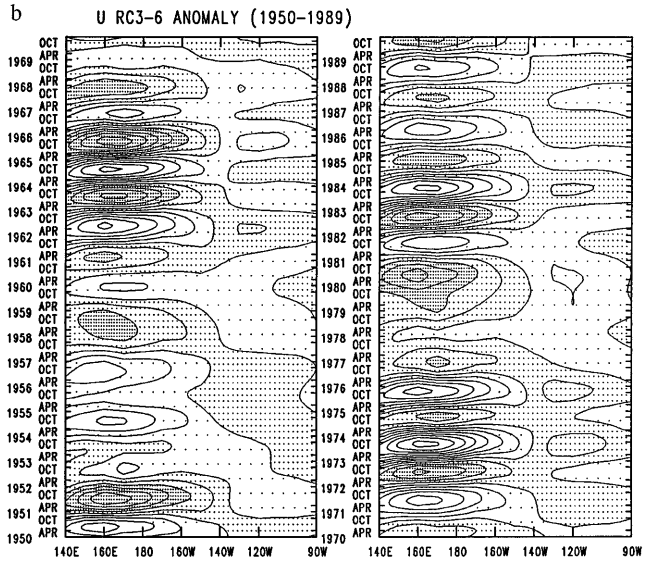

Fig. 7a, b. QB time series based on RCs 3–6 for **a** SST and **b** U. Contours and stippling as in Fig. 6.

7a) has its maximum located around 120°W, as for the QQ mode. A slight westward migration of the anomaly features across the eastern and central Pacific may also be seen (as in the eigenvectors of Fig. 5b). The correlation of the NINO-3 SST index from the RCs in Fig. 7a with the original time series is 0.67. The reconstructed QB variance contributes 18.4% to the NINO-3 variance. The QB may be regarded, therefore, as another fundamental ENSO mode, in addition to the QQ. This finding is consistent with the study of Rasmusson et al. (1990) to some extent, although they emphasized the role of the QB, whereas we find this to be secondary to the QQ.

The wind anomaly (Fig. 7b) shows consistent eastward migration of its features across the western and central Pacific, to the west of 160°W. This feature is consistent with the description of the QB mode by Rasmusson et al. (1990). Large-amplitude wind anomalies cover a smaller region than for the QQ mode.

4.3 The 15–16-month oscillation

SST anomalies associated with the 15–16-month oscillation (Fig. 8a) are quite consistent in their westward propagation across the eastern and central Pacific. The

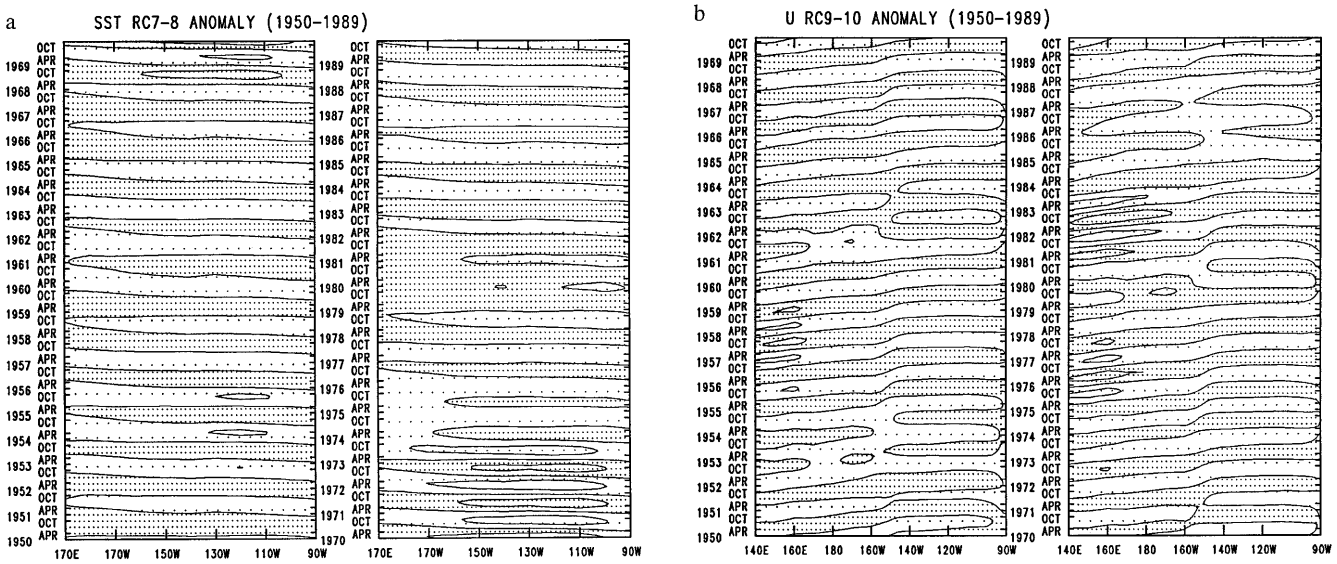

Fig. 8a, b. 15-month oscillation reconstructed from **a** RCs 7–8 for SST and **b** RCs 9–10 for U

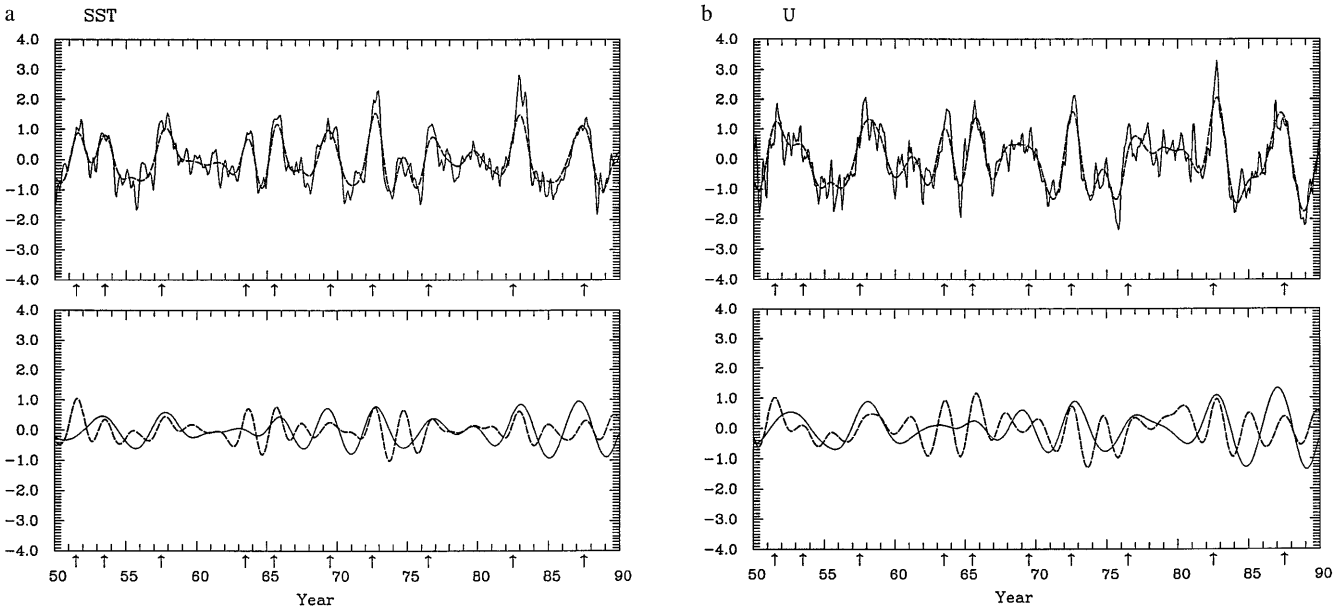

Fig. 9. a *Upper panel:* SST anomalies in the eastern equatorial Pacific "NINO-3" region (150°W–90°W) from the original time series (*solid line*) and the reconstructed QQ plus QB time series (*dashed line*). *Lower panel:* contribution of the QQ (RC 1–2; *solid line*) and QB (RC 3–6; *dashed line*) components. **b** As in **a** but for surface zonal wind anomalies in the western equatorial Pacific (140°E–160°W)

amplitude is much smaller than those of the two major interannual oscillations. The zonal wind (Fig. 8b) has the langest amplitude in the western Pacific, as with the QQ and QB oscillation. A slight tendency to eastward propagation may be seen, but since the spells of largest wind variation do not match well those in SST, we cannot place great confidence in the details of the spatial structure.

4.4 Superposition of QQ and QB contributions

Adding together the QQ and QB reconstructions (equivalent to RCs 1–6) for both SST and wind (not shown) yields multivariate time series that appear similar to the original, unfiltered ones in terms of accounting for major warm and cold events. To provide a clear view of this superposition, following Rasmusson et al. (1990) and Barnett (1991), Fig. 9 shows univariate time series averaged over two key regions for SST and wind, respectively. The correlation between the reconstructed NINO-3 time series and observed SST is 0.91. Bearing in mind that no band-pass prefiltering whatsoever was performed, this substantial correlation shows the very strong contribution of the combined QQ and QB modes to ENSO. Most El Niño episodes during the period coincide with the "warm" phase of

both modes, i.e., 1957, 1972, and 1982. Some ENSO episodes appear to be due to one mode alone, i.e., 1951 and 1963. It is noteworthy that the individual QQ series for wind and SST tend to behave similarly, despite the separate treatment of the two fields. The same remark holds for the two QB series.

4.5 Sensitivity tests to M-SSA parameters

To check the results presented so far, the robustness of the analysis was tested by repeating it with various other choices of window size and channel number. In particular, systematic analysis was carried out for alternate window lengths, of 75 and 90 months, and an alternate number of channels, 21, in the domain 170°E–90°E (corresponding to a sample rate of 5° longitude). The features of these results (not shown) are very similar to those presented here. The main difference is that, with more spatial channels, the signal in the RCs of the QQ and QB components is slightly weaker; this difference is clearly due to the attempt to capture more spatial detail from the same length of time series.

The order of the MEM analysis was also varied; when a very high order is used (roughly 60 or greater), spurious peaks can appear, but for order 15 to 45, the results (not shown) are much like those presented so far, for order 30. In particular, the periods of the major peaks are stable.

5 Annual cycle

The M-SSA analysis was repeated with the seasonal cycle included in the time series. This cycle will obviously dominate the temporal variability, but the space-time evolution along the equator of the annual cycle itself is a subject of current investigation in ocean-atmosphere interaction (Mechoso et al. 1995; Robertson et al. 1995a). Since the amount of data is very limited, one does not expect to resolve the interannual variability as well as when the seasonal cycle is removed, but it is still of interest whether the oscillations are robustly detected in the presence of this large additional signal.

The major results are listed in Table 2. The first pair (1–2), representing the annual cycle, stands out strongly in the spectra of eigenvalues for the combined SST-U case (Fig. 10). The second pair (3–4) and the third pair (5–6) also rise above the remaining eigenvalues and the noise spectrum. The power spectra obtained by using MEM for this combined SST-U case are shown for the six leading PCs (Fig. 11). The leading pair, 1–2, has a very sharp peak as expected for the highly periodic annual cycle. The second pair, 3–4, gives a clear peak at just over 4 years, in agreement with the QQ mode of Sect. 3 and 4.1, where the annual cycle had been subtracted. The peaks associated with PCs 5–6 have periods of just over two years, although the spectra of the two are not quite the same. The fact that the QQ and QB modes can still be clearly seen indicates that these two oscillations are highly robust in the equatorial Pacific region.

Table 2. As in Table 1, but for the case with seasonal cycle included in the analysis

Variables	Pair	Period (months)	Variance (%)
SST	1–2	12	34.1
	3–4	50	23.7
	5–6	27	11.9
U	1–2	12	22.9
	3–4	53	15.3
	5–6	28	10.0
SST-U combined	1–2	12	29.0
	3–4	53	19.2
	5–6	28	10.0

The structure of the annual cycle in space and in time lag, as represented by the associated eigenvectors, is shown in Fig. 12. Its largest amplitude is located in the eastern Pacific, as expected, and the corresponding EOFs are in perfect quadrature with each other. A distinct westward propagation is captured neatly in both SST and wind fields, in agreement with Horel (1982) and Philander and Chao (1991).

6 Summary and discussion

In order to examine modes of interannual variability, in the combined time-and-space domain, we performed multi-channel singular spectrum analysis (M-SSA) on COADS fields of equatorial SST and surface zonal wind, U, from 1950 to 1990. Three significant interannual oscillations are present, whether SST and U are analyzed separately or jointly. The major spectral peaks are at 52, 28, 24, and 15 months; the first corre-

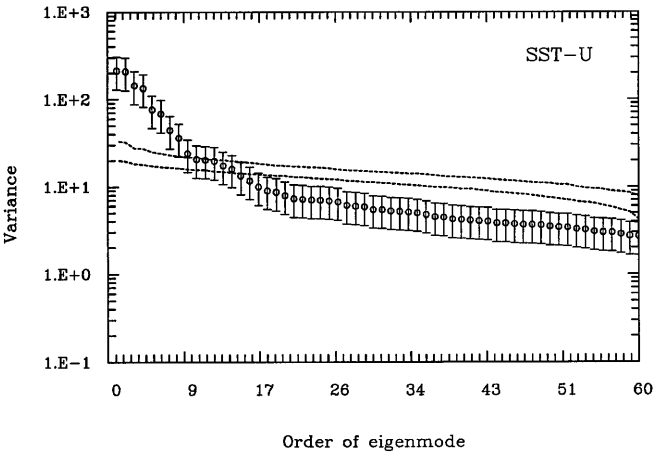

Fig. 10. M-SSA eigenvalue spectra of the calculations with the seasonal cycle included for the combined SST-U case, up to order 60, with error bars indicating the 95% confidence interval, plus a 95% confidence interval from a sample of 100 Monte Carlo white-noise realizations (*dashed line*)

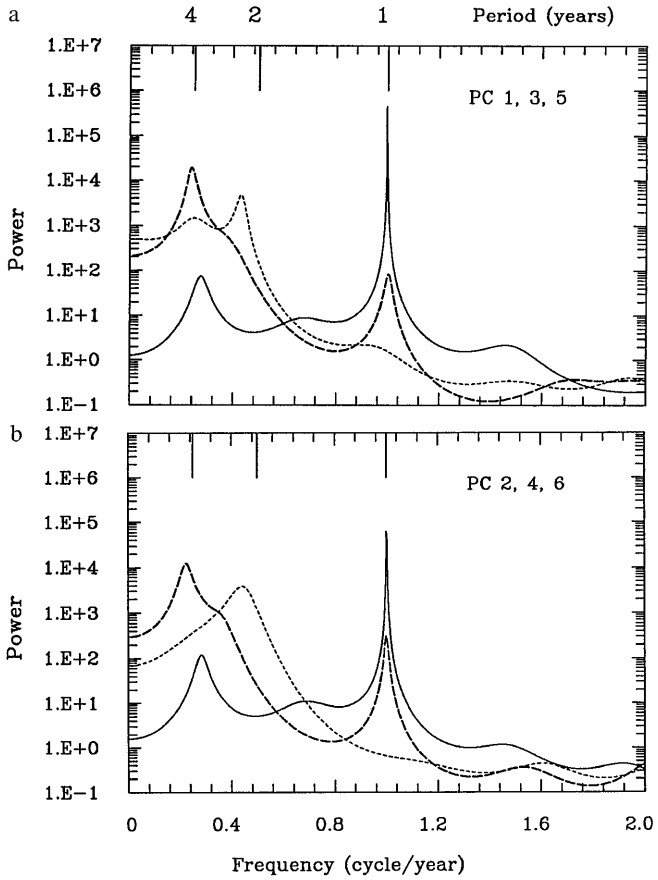

Fig. 11a, b. MEM spectra of PCs 1–6 of the calculations with the seasonal cycle included for the combined SST-U case; same convention as in Fig. 2

sponds to a *quasi-quadrennial* (QQ) oscillation, while the second and third appear to form a *quasi-biennial* (QB) oscillation. The QQ mode is a refinement of the "low-frequency" mode mentioned by Rasmusson et al. (1990). The analysis here defines the associated spectral peak more sharply and identifies this mode closely with ENSO. The terminology for the QB mode follows earlier authors. The 15–16-month oscillation is new, but is at the limit of what we can reliably detect and describe.

Despite the great attention paid to the tropical QB variability in recent studies (Rasmusson et al. 1990; Ropelewski et al. 1992), the QQ mode has the larger variance. The associated pair of eigenvalues is statistically significant in all cases computed: separate SST and U or combined SST-U fields; with the annual cycle removed or not; and for various choices of lag window. We are thus compelled to consider the QQ mode as more fundamental, because it is sharper, stronger and more statistically significant than the QB variability. In a time-longitude reconstruction of the QQ component, the SST has the form of a standing oscillation with large-scale anomalies throughout the eastern equatorial Pacific; the U field is dominated by a standing oscillation pattern in the western Pacific but also exhibits slight propagation to the east, through the central Pacific.

The fact that the QB variability is broken into two pairs of modes in this analysis suggests that it is spread over a broader frequency band or else is less robust than the QQ. The 28-month pair appears and is statistically significant in all cases. The pairing of eigenvalues for the 24-month oscillation, however, is not always statistically significant. The case for a single well-defined QB phenomenon with a clear spectral peak is thus much less conclusive than for the QQ oscillation. In reconstructing time-longitude series for the QB oscillation, we combine the 28-month and 24-month pairs. The locations of maximum anomalies are similar to those of the QQ mode. Slight westward migration in SST and eastward propagation of U in the region west of 160°W are found. The region with wind anomalies of significant amplitude has smaller extent than for the QQ oscillation.

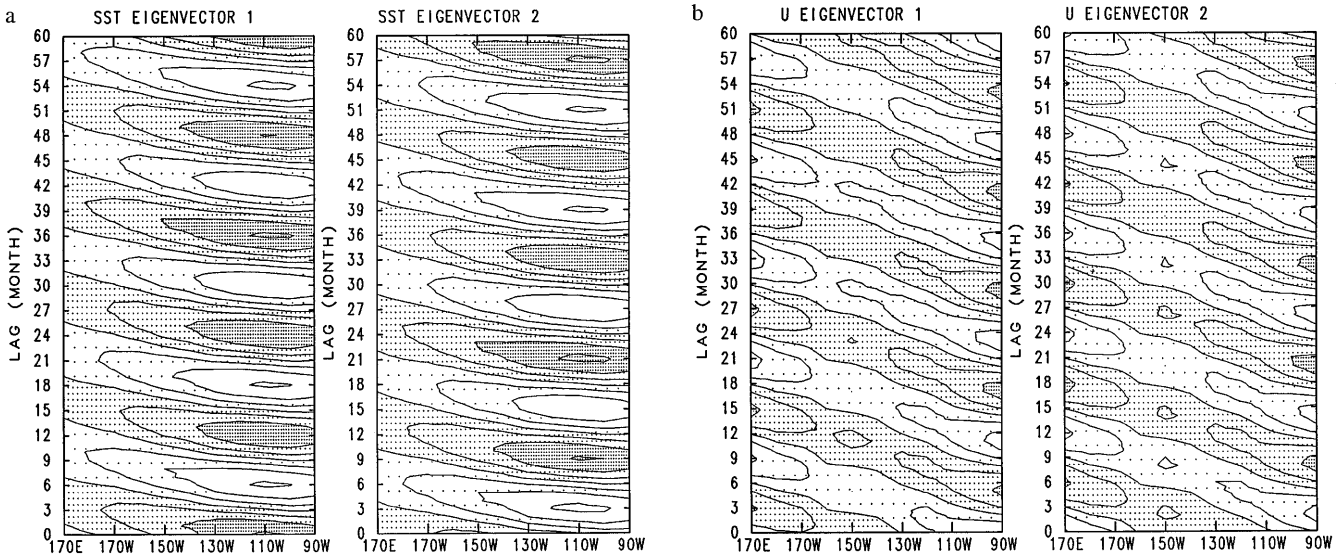

Fig. 12a, b. The equatorial Pacific seasonal cycle, as represented by M-SSA EOFs 1 and 2 for **a** SST and **b** U. Contour interval 0.025 for normalized eigenvectors (no units), *darkest stippling* for regions over 0.05, *no stippling* regions less than –0.05

The 15–16-month oscillation has smaller amplitude than the two major oscillations. The SST exhibits consistent westward propagation and the zonal wind shows eastward propagation in the western Pacific, although the two fields do not agree as well as for the two major modes in their evolution. Li (1994) found recently a similar 15-month oscillation in a monsoon index, the difference between wind at 850 mb and 200 mb averaged over the region (0°–20°N, 40°–110°E). Still, its identification here is tentative because of the small amplitude. Even so, this mode has a very suggestive interpretation in terms of the nonlinear interaction of the dominant QQ cycle and the annual cycle: such an interaction will produce power at the difference of the two primary frequencies, $(12 \text{ months})^{-1}$ and $(52 \text{ months})^{-1}$, yielding $(15.6 \text{ months})^{-1}$.

When the seasonal cycle is included in the M-SSA analysis, it becomes the leading mode, which exhibits westward propagation of SST andU along the equator. The coherent propagation of both fields in this annual mode indicates that the method can neatly capture propagating features. The occasional, apparent propagation noted for certain warm events (e.g., Gill and Rasmusson 1983) or for the Rasmusson and Carpenter (1982) composites does not appear sufficiently similar from one event to another to leave a truly decisive mark on the interannual modes. This is consistent with the idea that subsurface dynamical adjustment plays a large role in providing the memory of the oscillation during part of the cycle, with an essentially standing oscillation in SST (as seen, for instance, in the POP analysis of Latif et al. 1993 or in several ENSO models, including Cane and Zebiak 1985, as reviewed by Neelin et al. 1994).

While Jin and Neelin (1993) noted that characteristics of both propagation and standing SST oscillation could coexist within the same coupled mode in varying degrees, the propagating aspects are clearly less important in the observed interannual modes than in certain coupled GCMs (e.g., Meehl 1990; Lau et al. 1992). The westward SST propagation in the QB mode appears intriguing but is not accompanied by coherent westward propagation in wind. M-SSA analysis of 45 years simulated by a coupled GCM with no flux corrections (Robertson et al. 1995a, b) has yielded QQ and QB modes with similar characteristics. On the other hand, the westward propagation in the annual cycle could potentially be consistent with the westward-propagating mechanisms found in simple coupled models (e.g., Neelin 1991; Hao et al. 1993).

The reconstructed evolution of SST and U fields, based on QQ plus QB modes, provides a very good approximation to the ENSO time series. The overall correlation between the reconstructed time series and observed SST is 0.91, and all major ENSO events coincide with the QQ and QB modes interfering constructively. The importance of the superposition of the two modes supports and refines similar results obtained by Barnett (1991), who based his analysis on band-pass filtering in a priori, fixed low-frequency and QB bands. Barnett (1991) further estimated a rough measure of nonlinear interaction between these bands. The more sharply defined time scale of the QQ mode found here is particularly suggestive of possible interactions with the QB and the annual cycle, although this remains to be further quantified.

Possible scenarios for producing multiple interannual spectral peaks include the following : (1) the QQ and QB could be separate oscillations, generated by differing physics, each with an independent frequency; (2) the QQ mode might arise by period doubling from the QB; and (3) the interaction of the seasonal cycle and the fundamental ENSO frequency can nonlinearly entrain this frequency to a rational multiple of the annual frequency and produce additional peaks by combination tones. The second scenario was illustrated by Cane et al. (1990) and Münnich et al. (1991). The third was shown to occur in an intermediate ENSO model by Jin et al. (1994) and in a simple ENSO model by Tziperman et al. (1994).

The results presented here do help us distinguish between these scenarios, within the limitations arising from the short length of the time series available. The fact that the variance associated with the QQ is actually larger than that associated with the QB essentially rules out period doubling as an explanation of ENSO irregularity, since that scenario would imply a QB peak that is larger than the QQ peak. The similarity of the spatial structures of the QQ and QB tends to weigh against the hypothesis of different physics producing two independent frequencies; this is less conclusive, however, since we cannot examine the corresponding subsurface oceanic variables. The closeness of the QQ and QB peaks to integer multiples of the annual period, on the other hand, and the presence of the 15–16-month peak that approximates well a (4/3)-year period in the results shown here are all consistent with subharmonic frequency locking. In this scenario, the QQ would be the fundamental ENSO mode and its interactions with the seasonal cycle would tend to lock it to a four-year period, producing QB and (4/3)-year periods as a by-product of the nonlinear resonance.

Appendix

Multi-channel singular spectrum analysis (M-SSA)

Consider a finite, discrete data set consisting of a multi-channel time series X_{li}, $1 \le i \le N$, $1 \le l \le L$, with i representing time, l the channel number, and $X_{li} = X_l(i\tau_s)$ where τ_s is the sampling interval (Broomhead and King 1986b; Kimoto et al. 1991; Plaut and Vautard 1994). The mean is removed from the series. In the present application, the index l stands for the discrete longitude of an area average.

The M-SSA expansion of the data vectors X_{li}, $1 \le l \le L$, $1 \le i \le N$, onto an orthonormal basis is:

$$X_{l,i+j} = \sum_{k=1}^{L \times M} a_i^k E_{lj}^k, \qquad 1 \le l \le L, 1 \le j \le M.$$

Here the $L \times M$ state vector considered at time i is $(X_{1,i+1}, X_{1,i+2}, ..., X_{1,i+M}, X_{2,i+1}, ..., X_{2,i+M}, X_{L,i+1}, ..., X_{L,i+M})$. The coefficient a_i^k is called the k-th principal component (PC hereafter), M is the window size, and the embedding dimension is $L \times M$. The k-th basis vector E^k is the eigenvector of the block-Toeplitz $(L \times M) \times (L \times M)$ matrix T_X, containing the cross-covariance coefficients of the different channels l at lags 0 to $M-1$:

$$T_X = \begin{bmatrix} T_{11} & T_{12} & \cdot & \cdot & \cdot & T_{1L} \\ T_{21} & T_{22} & \cdot & & & \cdot \\ \cdot & & \cdot & \cdot & & \cdot \\ \cdot & & & T_{ll} & T_{ll'} & \cdot \\ \cdot & & & & \cdot & \cdot \\ T_{L1} & \cdot & \cdot & \cdot & \cdot & T_{LL} \end{bmatrix};$$

here $T_{ll'}$ is the $M \times M$ lag-covariance matrix between channel l and channel l'. The least-biased estimate of the element in row j and column j' of $T_{ll'}$, cf. Vautard et al. (1992), is:

$$(T_{ll})_{jj'} = \frac{1}{N - |j-j'|} \sum_{i=1}^{N-|j-j'|} x_{l,i} x_{l',i+j-j'}.$$

The k-th reconstructed component (RC hereafter), at time i and for channel l, is given by:

$$X_{li}^k = \frac{1}{i} \sum_{j=1}^{i} a_{i-j}^k E_{lj}^k, \quad \text{when } 1 \le i \le M-1,$$

$$X_{li}^k = \frac{1}{M} \sum_{j=1}^{M} a_{i-j}^k E_{lj}^k, \quad \text{when } M \le i \le N-M+1,$$

$$X_{li}^k = \frac{1}{N-i+1} \sum_{j=i-N+M}^{M} a_{i-j}^k E_{lj}^k, \quad \text{when } N-M+2 \le i \le N.$$

This is an average over M reconstruction estimates and is optimal in a least-square sense (Ghil and Vautard 1991; Vautard et al. 1992). Unlike PCs, which are scalar series, RCs are multi-channel series, representing the part of the original signal that corresponds to the associated eigenelements.

Acknowledgements. An earlier version of part of this work appeared in Jiang et al. (1993). It was supported by a grant from the Department of Energy's National Institute for Global Environmental Change (NJ, JDN, and MG) and by the National Oceanographic and Oceanic Administration Climate and Global Change Program Grants NA26GP0114/NA46GP0244 (JDN and NJ) and NA16RC0058 (MG). Computational equipment was provided by the Digital Equipment Corporation under the Sequoia 2000 project.

References

Barnett TP (1983) Interaction of the monsoon and Pacific trade wind system at interannual time scales. Part I: the equatorial zone. Mon Weather Rev 111:756–773

Barnett TP (1988) Variations in near-global sea level pressure: another view. J Clim 1:225–230

Barnett TP (1991) The interaction of multiple time scales in the tropical climate system. J Clim 4:269–285

Bernardet P, Butet A, Déqué M, Ghil M, Pfeffer RL (1990) Low-frequency oscillations in a rotating annulus with topography. J Atmos Sci 47:3023–3043

Broomhead DS, King GP (1986a) Extracting qualitative dynamics from experimental data. Physica D 20:217–236

Broomhead DS, King GP (1986b) On the qualitative analysis of experimental dynamical systems. In: Sarkar S (ed) Nonlinear phenomena and chaos. Adam Hilger, Bristol, pp 113–144

Cane M, Zebiak SE (1985) A theory for El Niño and the Southern Oscillation. Science 228:1084–1087

Cane M (1986) El Niño. Annu Rev Earth Planet Sci 14:43–70

Cane M, Münnich M, Zebiak SE (1990) A study of self-excited oscillations of the tropical ocean-atmosphere system. Part I: linear analysis. J Atmos Sci 47:1562–1577

Dettinger MD, Ghil M, Strong CM, Weibel W, Yiou P (1995) Software expedites singular-spectrum analysis of noisy time series. Eos, Trans Am Geophys Un 76:12, 14, 21

Dickey JO, Marcus SL, Hide R (1992) Global propagation of interannual fluctuations in atmospheric angular momentum. Nature 375:485–488

Ghil M, Mo K (1991) Intraseasonal oscillations in the global atmosphere. Part I: Northern Hemisphere and tropics. J Atmos Sci 48:752–779

Ghil M, Vautard R (1991) Interdecadal oscillations and the warming trend in global temperature time series. Nature 350:324–327

Gill AE, Rasmusson EM (1983) The 1982–1983 climate anomaly in the equatorial Pacific. Nature 306:229–234

Hao Z, Neelin JD, Jin FF (1993) Nonlinear tropical air-sea interaction in the fast-wave limit. J Clim 6:1523–1544

Hasselmann K (1988) PIPs and POPs : the reduction of complex dynamical systems using principal interactions patterns and oscillation patterns. J Geophys Res 93:11015–11021

Horel JD (1982) The annual cycle in the tropical Pacific atmosphere and ocean. Mon Weather Rev 110:1863–1878

Horel JD (1984) Complex principal component analysis: theory and examples. J Clim Appl Meteorol 23:1660–1673

Jiang N, Neelin JD, Ghil M (1993) Quasi-quadrennial and quasi-biennial variability in COADS equatorial Pacific sea surface temperature and zonal wind. Proc 17th Clim Diagn Workshop. Climate Analysis Center, NOAA, 348–353

Jin FF, Neelin JD (1993) Modes of interannual tropical ocean-atmosphere interaction – a unified view. Part I: numerical results. J Atmos Sci 50:3477–3503

Jin FF, Neelin JD, Ghil M (1994) El Niño on the "Devil's Staircase": Annual subharmonic steps to chaos. Science 264:710–713

Keppenne C, Ghil M (1992a) Extreme weather events. Nature 358:547

Keppenne C, Ghil M (1992b) Adaptive filtering and prediction of the Southern Oscillation index. J Geophys Res 97:20449–20454

Kimoto M, Ghil M, Mo KC (1991) Spatial structure of the 40-day oscillation in the Northern Hemisphere extratropics. Proc 8th Conf Atmos & Oceanic Waves & Stability. American Meteorological Society, Boston, pp 115–116

Latif M, Sterl A, Maier RE, Junge MM (1993) Structure and predictability of the El Niño/Southern Oscillation phenomenon in a coupled ocean-atmosphere general circulation model. J Clim 6:700–708

Lau KM, Sheu PJ (1988) Annual cycle, quasi-biennial oscillation and Southern Oscillation in global precipitation. J Geophys Res 93:10975–10988

Lau NC, Philander SGH, Nath MJ (1992) Simulation of El Niño/Southern Oscillation phenomena with a low-resolution coupled circulation model of the global ocean and atmosphere. J Clim 5:284–307

Li CF (1994) Interannual variability of Asian Summer Monsoon and its relationships with ENSO and Eurasian Snow Cover. Ph. D. Dissertation, University of California, Los Angeles

Mechoso CR, Robertson AW, Barth N, Davey MK, Delecluse P, Gent PR, Ineson S, Kirtman B, Latif M, Le Treut H, Nagai T, Neelin JD, Philander SGH, Polcher J, Shopf PS, Stockdale T, Suarez MJ, Terray L, Thual O, Tribbia JJ (1995) The seasonal

cycle over the tropical Pacific in coupled ocean-atmosphere general circulation models. Mon Weather Rev 123:2825–2838

Meehl GA (1987) The annual cycle and interannual variability in the tropical Pacific and Indian Ocean regions. Mon Weather Rev 115:27–50

Meehl GA (1990) Seasonal cycle forcing of El Niño/Southern Oscillation in a global coupled ocean-atmosphere GCM. J Clim 3:72–98

Münnich M, Cane M, Zebiak SE (1991) A study of self-excited oscillations of the tropical ocean-atmosphere system. Part II: nonlinear cases. J Atmos Sci 48:1238–1248

Neelin JD (1991) The slow sea surface temperature mode and the fast-wave limit: analytic theory for tropical interannual oscillations and experiments in a hybrid coupled model. J Atmos Sci 48:584–606

Neelin JD, Latif M, Jin FF (1994) Dynamics of coupled ocean-atmosphere models: the tropical problem. Annu Rev Fluid Mech 26:617–659

Penland MC, Ghil M, Weickmann K (1991) Adaptive filtering and maximum entropy spectra with application to changes in atmospheric angular momentum. J Geophys Res 96:22659–22671

Philander SGH (1990) El Niño, La Niña, and the Southern Oscillation. Academic Press, San Diego

Philander SGH, Chao Y (1991) On the contrast between the seasonal cycles of the equatorial Atlantic and Pacific Oceans. J Phys Oceanogr 21:1399–1406

Plaut G, Vautard R (1994) Spells of oscillations and weather regimes in the low-frequency dynamics of the Northern Hemisphere. J Atmos Sci 51:210–236

Preisendorfer RW (1988) Principal Component Analysis in Meteorology and Oceanography. Mobley CD (ed) Elsevier, Amsterdam

Quinn W, Zopf D, Short K, Yang R (1978) Historical trends and statistics of the Southern Oscillation, El Niño, and Indonesian drought. Fisheries Bull 76 (3):663–678

Rasmusson EM, Carpenter TH (1982) Variations in tropical sea surface temperature and surface wind fields associated with the Southern Oscillation/El Niño. Mon Weather Rev 110:354–384

Rasmusson EM, Wang X, Ropelewski CF (1990) The biennial component of ENSO variability. J Mar Syst 1:71–96

Robertson A, Ma CC, Mechoso CR, Ghil M (1995a) Simulation of the tropical Pacific climate with a coupled ocean-atmosphere general circulation model. Part I: the seasonal cycle. J Clim 8:1178–1198

Robertson A, Ma CC, Ghil M, Mechoso CR (1995b) Simulation of the tropical Pacific climate with a coupled ocean-atmosphere general circulation model. Part II: interannual variability. J Clim 8:1199–1216

Ropelewski CF, Halpert MS, Wang X (1992) Observed tropospheric biennial variability in the global tropics. J Clim 5:594–614

Trenberth KE, Shin WT (1984) Quasi-biennial fluctuations in sea level pressure over the Northern Hemisphere. Mon Weather Rev 112:761–777

Tziperman E, Stone L, Cane M, Jarosh H (1994) El Niño chaos: overlapping of resonance between the seasonal cycle and the Pacific ocean-atmosphere oscillator. Science 264:713–715

Unal YS, Ghil M (1995) Interannual and interdecadal oscillation patterns in sea level. Clim Dyn 11:255–278

Vautard R, Ghil M (1989) Singular spectrum analysis in nonlinear dynamics with applications to paleoclimatic time series. Physica D 35:395–424

Vautard R, Yiou P, Ghil M (1992) Singular spectrum analysis: A toolkit for short, noisy chaotic signals. Physica D 58:95–126